Optics Letters

Remote mid-infrared photoacoustic spectroscopy with a quantum cascade laser

Thomas Berer,[1,2,*] Markus Brandstetter,[1] Armin Hochreiner,[1] Gregor Langer,[2] Wolfgang Märzinger,[4] Peter Burgholzer,[1,2] and Bernhard Lendl[3]

[1]Research Center for Non-Destructive Testing GmbH (RECENDT), Altenberger Straße 69, 4040 Linz, Austria
[2]Christian Doppler Laboratory for Photoacoustic Imaging and Laser Ultrasonics, Altenberger Straße 69, 4040 Linz, Austria
[3]Institute of Chemical Technologies and Analytics, Vienna University of Technology, Getreidemarkt 9/164AC, 1060 Vienna, Austria
[4]i-RED Infrarot Systeme GmbH, Hafenstraße 47-51, 4020 Linz, Austria
*Corresponding author: thomas.berer@recendt.at

Received 6 May 2015; revised 25 June 2015; accepted 30 June 2015; posted 1 July 2015 (Doc. ID 240400); published 21 July 2015

We demonstrate non-contact remote photoacoustic spectroscopy in the mid-infrared region. A room-temperature-operated pulsed external-cavity quantum cascade laser is used to excite photoacoustic waves within a semitransparent sample. The ultrasonic waves are detected remotely on the opposite side of the sample using a fiber-optic Mach–Zehnder interferometer, thereby avoiding problems associated with acoustic attenuation in air. We present the theoretical background of the proposed technique and demonstrate measurements on a thin polystyrene film. The obtained absorption spectrum in the region of 1030–1230 cm^{-1} is compared to a spectrum obtained by attenuated total reflection, showing reasonable agreement.

OCIS codes: (300.0300) Spectroscopy; (120.0280) Remote sensing and sensors; (140.5965) Semiconductor lasers, quantum cascade; (280.1545) Chemical analysis; (110.5125) Photoacoustics.

http://dx.doi.org/10.1364/OL.40.003476

Mid-infrared (mid-IR) spectroscopy is a powerful analytical method that offers access to qualitative and quantitative chemical information of the sample under investigation. In classical absorption spectroscopy, light is attenuated by the sample and the remaining light is optically detected. In case of highly absorbing samples, optical detection can be challenging. A number of indirect detection schemes were developed to circumvent this issue. The majority of reported methods are based on photothermal effects, induced by absorption of mid-IR radiation [1]. Different relaxation mechanisms can take place, resulting, e.g., in blackbody radiation [2], refractive index change [3], or acoustic waves [4].

Photothermal and photoacoustic signals are proportional to the absorbed radiation, thus sensitivity can be improved by use of high-power excitation sources. Suitable excitation sources for the mid-IR spectral region are quantum cascade lasers (QCLs), semiconductor-based high-power mid-IR sources, which have evolved during the last two decades [5]. QCLs are available in various configurations optimized for different analytical tasks. The range stretches from narrow line-width distributed feedback QCLs (DFB-QCLs) for gas phase analysis [6] to ultra-broadband external-cavity QCLs (EC-QCL) for condensed-phase analysis [7]. In contrast to thermal emitters or optical parametric oscillators (OPOs), QCLs unite fast spectral tuning, high-frequency signal modulation, and high-power spectrally selective illumination of the target analyte.

In the present Letter, we introduce a new measurement concept for remote chemical analysis based on the photoacoustic effect. Mid-IR laser radiation of a spectrally tunable EC-QCL serves as pump source. The photoacoustic wave generated within the sample is remotely detected by a fiber-optic interferometer through the resulting surface deformation [8]. In this configuration, limitations usually seen when employing acoustic detection, such as attenuation of the acoustic wave in air, are circumvented. Thereby, much larger remote detection distances can be maintained.

A schematic of the used setup is depicted in Fig. 1. A room-temperature-operated pulsed EC-QCL (Daylight Solutions, USA) is focused onto a sample with lens L1 (zinc selenide, focal length 50 mm). The emission wavelength of the QCL is tunable over a spectral region from 1030 to 1230 cm^{-1}, i.e., from 8.12 to 9.71 μm. From the minimal beam diameter of 2.1 mm and a typical M^2 factor of 1.3, we calculated the diameter of the focal spot on the sample to be 320 μm and 380 μm, for wavenumbers of 1230 cm^{-1} and 1030 cm^{-1}, respectively. The QCL is operated at a repetition rate $f_R =$ 100 kHz and with its minimal pulse length of 40 ns. The laser emission power is maximum at 1180 cm^{-1} with 350 mW. For a pulse length of 40 ns, the respective pulse energy is 14 nJ. At 1230 cm^{-1} and 1030 cm^{-1}, the pulse energy decreases to about 9.1 nJ and 1.2 nJ, respectively. The corresponding radiant exposures for 1030 cm^{-1}, 1180 cm^{-1}, and 1230 cm^{-1} are 1 $\mu J/cm^2$, 16 $\mu J/cm^2$, and 11 $\mu J/cm^2$, respectively.

The absorption of the laser radiation within the sample leads to thermal expansion followed by generation of ultrasonic waves. The ultrasonic waves are detected on the opposite side of the sample by a vibrometer, based on a fiber optic interferometer. The interferometer is described in detail in [9]. In brief, light from a cw fiber laser at a wavelength of 1549.9 nm is split into a reference path and a detection path. Light from the latter path is focused onto the sample using a fiber collimator (Col) and a lens L2 with focal length of 75 mm, representing the current remote detection distance. Light that is reflected from the sample surface is collected by the same optics. Before combination with the reference path, the light is amplified by means of optical amplification (OA) using an erbium-doped fiber amplifier. The combined light interferes on a balanced photo detector. The working point of the interferometer is stabilized with a piezo-electric phase shifter (not shown in Fig. 1). Ultrasonic vibrations on the sample surface change the relative phase between reference and sample beam, thus the output of the photodetector is directly related to the surface displacements. As the ultrasonic displacements are small, the output of the detector is coupled to a lock-in amplifier (LIA, Stanford Research Systems SR844), locked at the repetition rate of the QCL, to enhance the signal/noise ratio (SNR). Thus, only the frequency component of the surface vibration at the repetition rate of the laser is measured, however, with a high SNR. For plane waves, the pressure is proportional to the time derivative of the surface displacement [8]. The LIA measures only a single spectral component of the displacement, i.e., a harmonic signal. The amplitude of the derivative of a harmonic signal is proportional to the amplitude of the signal. Thus, the output of the LIA is directly proportional to the pressure.

The intensity profile of the incident mid-IR laser radiation over depth is schematically indicated in Fig. 2(a). For short laser pulses, the pressure rise due to light absorption can be estimated by [10]

$$p_0 = \frac{\beta v^2}{c_p}\mu F = \Gamma \mu F, \tag{1}$$

where β is the isobaric volume expansion coefficient, v is the speed of sound, c_p is the specific heat, μ is the absorption coefficient, F is the fluence, and Γ is the Grüneisen parameter.

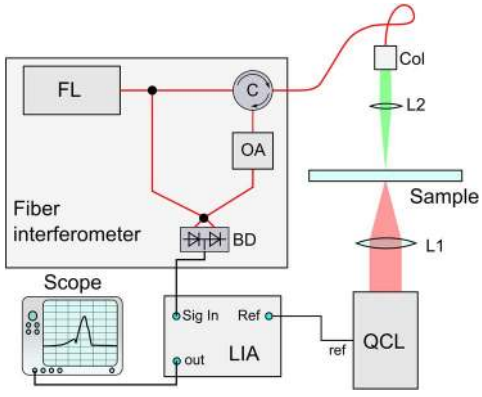

Fig. 1. Schematic of the setup with component labels given as: QCL, quantum cascade laser; FL, fiber laser; LIA, lock-in amplifier; BD, balanced photo detector; OA, optical amplifier; Col, fiber collimator; L1,2, lenses; C, circulator.

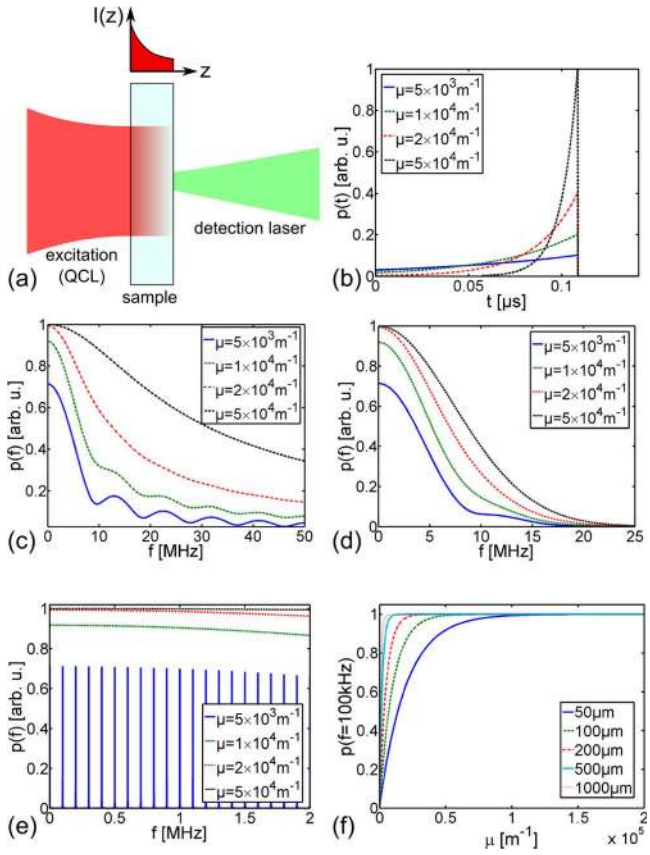

Fig. 2. (a) Light from the QCL (left, red) is absorbed in a sample. The intensity as a function over depth is indicated above the sample. Ultrasonic waves are detected at the opposite side (right, green). (b) Resulting pressure over time for a sample thickness of 250 μm and different absorption coefficients neglecting reflections. (c) Spectral components of the time traces in (b). (d) Spectral components taking the pulse length of the excitation pulse into account. (e) Spectral components for a repetitive excitation with a pulse train for $\mu = 5 \times 10^3$ m^{-1} (blue) and envelope functions for the other absorption values. (f) Amplitudes evaluated at 100 kHz over absorption coefficient μ for different sample thicknesses.

From Beer–Lambert law, we find the generated pressure over the sample depth z to be [10]

$$p_0(z) = \Gamma \mu F \exp(-\mu z). \tag{2}$$

The generated pressure wave is then propagating through the media. If the sample thickness is smaller than the diameter of the excitation spot, one can assume the propagating wave to be approximately a plane wave. Neglecting reflections we find the pressure over time t at the detection surface to be:

$$p(t) \propto \mu \cdot e^{-\mu d} \cdot e^{\mu v t}\theta(d/v - t)\theta(t), \tag{3}$$

where d is the sample thickness, and θ denotes the Heaviside function. Calculated time traces of $p(t)$ for different absorption coefficients, a sample thickness $d = 250$ μm, and a speed of sound of 2300 m/s are shown in Fig. 2(b). For $\mu = 5 \times 10^3$ m^{-1} and $\mu = 1 \times 10^4$ m^{-1}, the total energy contained within the laser pulses is only partly absorbed, i.e., the curves are not zero at $t = 0$, while for $\mu = 2 \times 10^4$ m^{-1} and $\mu = 5 \times 10^4$ m^{-1}, the pulses are almost completely absorbed

within the sample. To find the spectral response we calculate the Fourier transform of (3) and find:

$$p(f) \propto \mu \frac{e^{-i2\pi f d/v} - e^{-\mu d}}{\sqrt{2\pi}(\mu v - i2\pi f)}. \quad (4)$$

The respective frequency domain spectra for the values used in Fig. 2(b) are shown in Fig. 2(c) for frequencies up to 50 MHz. With increasing μ, the maximum amplitude of the spectrum increases, and the spectrum becomes broader. The latter is because the temporal profiles become narrower with increasing μ [compare to Fig. 2(b)]. The above calculations were made under the assumption of infinitely short excitation pulses. A common criterion for the validity of this assumption is the fulfillment of the stress confinement condition [10], i.e., the pulse length has to be shorter than the sample thickness divided by the speed of sound. For the pulse length of 40 ns used during the experiments, stress confinement is fulfilled for sample thicknesses larger than 100 μm. However, also if the stress confinement condition is fulfilled, high frequencies may not be excited. The signal shape for arbitrary pulses can be calculated by convoluting the signal excited with a short pulse with the temporal profile of the excitation pulse. In frequency domain, this convolution corresponds to a multiplication. Figure 2(d) shows the resulting spectra, assuming the temporal shape of the pulse to be Gaussian. Due to the Gaussian pulse profile, high acoustic frequency components become less excited. The low-frequency response, however, does not change significantly. In particular, the amplitudes at the measurement frequency of 100 kHz are virtually unaffected. In the proposed setup, the spectral component of the ultrasonic pulse train at 100 kHz is evaluated with the LIA. A detailed explanation of the detection principle using a LIA to measure spectral components of repetitive excitations can be found, e.g., in [11]. In frequency domain, the pulse train can be calculated by summation over N individual pulses:

$$p_{\mathrm{tr}}(\omega) \propto p(\omega) \sum_{n=0}^{N-1} e^{-i\omega \cdot n/f_R}, \quad (5)$$

where the time delay between the pulses is described by the exponential function, and $\omega = 2\pi f$ is the angular frequency. As result, the Fourier transform of a pulse train shows

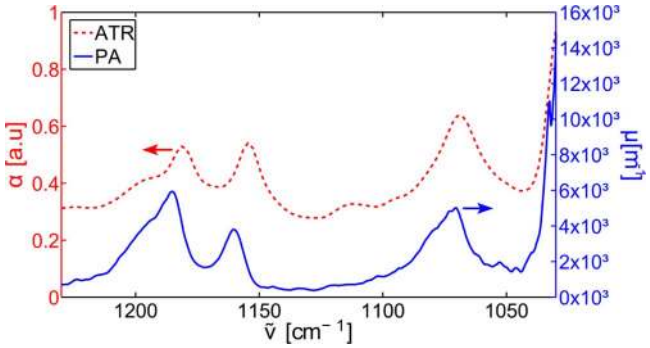

Fig. 3. Remote photo-acoustic measurement (blue solid line) of a polystyrene film and absorption data obtained from ATR (red dashed line) versus wavenumber. The measurements show reasonable agreement.

equidistant lines which are located at integer multiples of the laser repetition rate. The height of the peaks, i.e., the envelope, is given by the single-shot frequency components. In Fig. 2(e) the resulting spectrum is plotted for $\mu = 5 \times 10^3$ m^{-1}. For illustrative reasons, only the envelope is plotted for the other values of μ. One can see that for the higher absorption coefficients, i.e., in case the whole pulse is absorbed in the sample, the resulting low frequency components are nearly undistinguishable. This behavior is depicted in Fig. 2(f), showing the responses for $f_R = 100$ kHz over μ for different sample thicknesses. From Fig. 2(f), we see that above a certain value $\mu \cdot d$, the pressure signals begin to saturate. This behavior can be explained by calculating the approximate low-frequency response. For typical values, i.e., d in the range of several 100 μm, v around 2000 m/s, μ in the range of 10^4 m^{-1}, and a laser repetition rate of 100 kHz, we find that $\exp(-i2\pi f d/v)$ is close to one, and that $\mu v \gg \omega$. Finally, from Eq. (4) we find:

$$p(f_R = 100\ \mathrm{kHz}) \propto \frac{1 - e^{-\mu d}}{v}. \quad (6)$$

For small values of $\mu \cdot d$, the frequency component at f_R increases almost linearly with μ. For high values of $\mu \cdot d$, $(1 - \exp(-\mu d))$ converges to 1, and the frequency component saturates. In order to obtain significant results, the measurements should be performed in the non-saturated region of the curve. Thus, for many polymers and fluids, the method works best for maximum film thicknesses between 20 and 500 μm, depending on the maximum absorption coefficient.

We note that acoustic reflections arising from sample interfaces may contribute to the measurement signal. The spectrum of the signal including a reflection from the backside is given by

$$p_{\mathrm{bs}}(\omega) = p(\omega) - p^*(\omega) \cdot \chi \cdot e^{-i\omega 2d/v}, \quad (7)$$

where p^* is the conjugate complex of p, and χ is a factor between 0 and 1, describing the reduced amplitude due to reflection, spatial propagation, and attenuation. Multiple reflections (number of reflections >1) can be described similarly to Eq. (5) by

$$p_{\mathrm{mr}}(\omega) = p_{\mathrm{bs}}(\omega) \sum_m e^{-2i\omega d \cdot m/v} \cdot \chi^{2m}. \quad (8)$$

When calculating the low-frequency response of Eq. (8), one finds that the approximation in Eq. (6) is still valid, also for the case of multiple reflections.

The measurement principle was demonstrated on the example of a polystyrene film. For the remote photoacoustic measurements, a 250-μm-thick polystyrene film was chosen. From attenuated total reflection (ATR) measurements, we found that the polystyrene sheet has a maximum absorption coefficient below 1.5×10^4 m^{-1} in the spectral region defined by the excitation source. For the measurement, the LIA was locked to the pulse repetition rate of the QCL using its reference output. Data were acquired with the time constant of the LIA set to 100 ms; one spectral scan was obtained within 7.3 s. The analog output of the LIA was sampled with an 8-bit digital scope (LeCroy WaveRunner 44Xi-A). To increase the SNR, 16 subsequent scans were averaged. The data were then normalized to the emission spectrum of the QCL, given in [12]. The absorption coefficient μ was calculated from the normalized pressure

data using Eq. (4). The results of the measurement are shown in Fig. 3 (blue solid curve). For comparison, data obtained with an FTIR spectrometer using an ATR accessory (single reflection, diamond ATR) are plotted (red dashed curve). In the ATR spectrum, band positions are slightly shifted toward lower wavenumbers. Also the relative band intensities appear higher at lower wavenumbers. These effects are in accordance to the ATR theory and are caused by the wavelength dependency of the penetration depth and by the change in refractive index at the absorption bands [13,14].

In conclusion we demonstrated remote photoacoustic spectroscopy in the mid-IR. Ultrasonic waves were excited by pulses from a QCL. The generated ultrasonic waves were detected remotely on the opposite side of the sample using a fiber-optic interferometer coupled to a LIA. We presented the theoretical concept of the technique and demonstrated measurements on a polystyrene sheet. In the current setup, excitation and detection were done from opposite sides of the sample. However, excitation and detection can also be done from the same side, which may be more practical in real-life applications. The distance between sample and vibrometer can be increased by changing the focusing optics. We plan to extend the detection range to several meters and the combination with scanning optics presented in [15] to achieve laterally resolved chemical information of the sample under investigation. Hyperspectral imaging using nanospectroscopy was, e.g., reported in [16]. Therein, a spatial resolution below 50 nm was achieved by using an atomic force microscope. In the setup presented here, the spatial resolution is limited by the spot size of the detection laser, which is 10 μm in the current implementation. A spot diameter down to about 1 μm could be realized by tightly focusing the detection beam to a diffraction limited spot. In this case, however, the detection distance has to be reduced, thereby trading the advantage of a distant measurement against resolution.

Funding. Austrian Science Fund (FWF) (P25584-N20); Christian Doppler Research Association (Christian Doppler Laboratory for Photoacoustic Imaging and Laser Ultrasonics); Federal Ministry of Economy, Family and Youth, the European Regional Development Fund (EFRE); Federal State Upper Austria and the Austrian Research Funding Association (FFG) (843546).

REFERENCES

1. H. Coufal, Fresenius Z. Anal. Chem. **324**, 456 (1986).
2. X. Guo, A. Mandelis, and B. Zinman, J. Biophotonics **6**, 911 (2012).
3. R. H. Farahi, A. Passian, L. Tetard, and T. Thundat, J. Phys. D **45**, 125101 (2012).
4. J. P. Waclawek, R. Lewicki, H. Moser, M. Brandstetter, F. K. Tittel, and B. Lendl, Appl. Phys. B **117**, 113 (2014).
5. Y. Yao, Y. Yao, A. J. Hoffman, and C. F. Gmachl, Nat. Photonics **6**, 432 (2012).
6. M. T. McCulloch, E. L. Normand, N. Langford, G. Duxbury, and D. A. Newnham, J. Opt. Soc. Am. B **20**, 1761 (2003).
7. A. Hugi, R. Terazzi, Y. Bonetti, A. Wittmann, M. Fischer, M. Beck, J. Faist, and E. Gini, Appl. Phys. Lett. **95**, 061103 (2009).
8. T. Berer, A. Hochreiner, S. Zamiri, and P. Burgholzer, Opt. Lett. **35**, 4151 (2010).
9. A. Hochreiner, J. Bauer-Marschallinger, P. Burgholzer, B. Jakoby, and T. Berer, Biomed. Opt. Express **4**, 2322 (2013).
10. M. Xu and L. V. Wang, Rev. Sci. Instrum. **77**, 041101 (2006).
11. G. Langer, K.-D. Bouchal, H. Grün, P. Burgholzer, and T. Berer, Opt. Express **21**, 22410 (2013).
12. M. Brandstetter and B. Lendl, Sens. Actuators B **170**, 189 (2010).
13. J. M. Chalmers and P. R. Griffiths, *Handbook of Vibrational Spectroscopy* (Wiley, 2001), p. 4000.
14. G. Ramer and B. Lendl, *Encyclopedia of Analytical Chemistry* (Wiley, 2013).
15. E. Leiss-Holzinger, J. Bauer-Marschallinger, A. Hochreiner, P. Hollinger, and T. Berer, "Dual modality non-contact photoacoustic and spectral domain OCT imaging," Ultrasonic Imaging, doi: 10.1177/0161734615582003 (to be published).
16. F. Lu and M. A. Belkin, Opt. Express **19**, 19942 (2011).